JETIR.ORG ISSN: 2349-5162 | ESTD Year : 2014 | Monthly Issue
JOURNAL OF EMERGING TECHNOLOGIES AND INNOVATIVE RESEARCH (JETIR)
An International Scholarly Open Access, Peer-reviewed, Refereed Journal

DYNAMIC BEHAVIOR OF MODIFIED CONFIGURATIONS OF CONSTANT FORCE SLIDER MECHANISMS

[1]Ikechukwu Celestine Ugwuoke, [2]Matthew Sunday Abolarin
[1]Associate Professor, [2]Professor
[1,2]Department of Mechanical Engineering, Federal University of Technology, Minna, Nigeria.

Abstract : This research addresses the desire to understand the dynamic behavior of all Modified Configurations of Constant Force Slider Mechanisms (CFSMs) developed. Based on the principle of Dynamic Equivalence, a Generalized Mathematical Dynamic Model (GMDM) was developed for all modified configurations of CFSMs. In the dynamic evaluation of the modified configurations of CFSMs, three useful plots were also analyzed, the mean force plots, the median force plots, and the peak-to-peak force magnitude difference plots as a function of frequency. The peak-to-peak force plots also revealed the same interesting phenomenon which indicated that there is a range of frequencies over which the modified configurations of CFSMs also exhibit better constant-force behavior than they do statically. This better constant-force behavior is also likely due to inertial effects as expressed by every other previous researcher. The results obtained from experimentation with the inclusion of $\boldsymbol{\tau_{CF}}$ and $\boldsymbol{\tau_{AF}}$ show a very good agreement with that from the GMDM. Over the range of frequencies tested, the results for the modeled force were also within 1% of the relative error of the measured force. Depending on what attributes are most desirable; a wide frequency range with moderately low peak-to-peak force, a single frequency with very low peak-to-peak force, or some other similar effects, the modified configurations of CFSM parameters can also be optimized to achieve the desired results.

IndexTerms **- Dynamic behavior, Modified configurations, Dynamic equivalence, Generalized dynamic model, Peak-to-peak force plot, Inertial effects, Experimentation.**

I. INTRODUCTION

Compliant Mechanisms (CMs) are mechanisms that utilize compliance of their constituent elements to transmit motion/or force. They are particularly suited for applications with a small range of motions [7]. The use of CMs will continue to increase with time as materials and design methodologies are improved. The largest challenge is the relative difficulty in analyzing and designing CMs. Knowledge of mechanism analysis and synthesis methods and the deflection of flexible members are required. The combination of the two bodies of knowledge in CMs requires not only an understanding of both but also an understanding of their interactions in a complex situation. Techniques such as finite element analysis (FEA) and elliptic integrals provide accurate information, but make design very drawn out and complicated. Fortunately, the development of the PRBM has greatly increased the speed and ease in which CMs can be designed [4]. The PRBM allows for the approximation of the force-deflection characteristics of flexible segments. It is intended to be an intermediate design tool, allowing for the rapid design and analysis of first generation CMs. Modified Compliant Constant Force Compression Mechanisms are basically compliant slider-crank mechanisms possessing a combination of both rigid and flexible segments. These class of mechanisms maintain a constant force regardless of input displacement which is accomplished by determining specific geometric ratios that allow for equal increases in stored strain energy and mechanical advantage.

Using type-synthesis techniques, Murphy [11], and Murphy *et al.* [10], generated 28 possible compliant slider-crank mechanism (CSCM) configurations that generate a constant output force for a wide range of input displacements. Type synthesis is concerned with predicting which combination of linkage topology and type of joints may be best suited to solve a particular task. Howell et al. [5] carried out the dimensional synthesis of several of these configurations. Figures 1 show the side by side comparison of the modified configurations of CFSMs with the original configurations. These configurations have been divided into 5 classifications based on the number of flexible segments and their location in each configuration [15]. To improve on the performance and operational accuracy of the modified configurations of CFSMs, both dynamic analysis and dynamic design of the CFSMs need to be further studied.

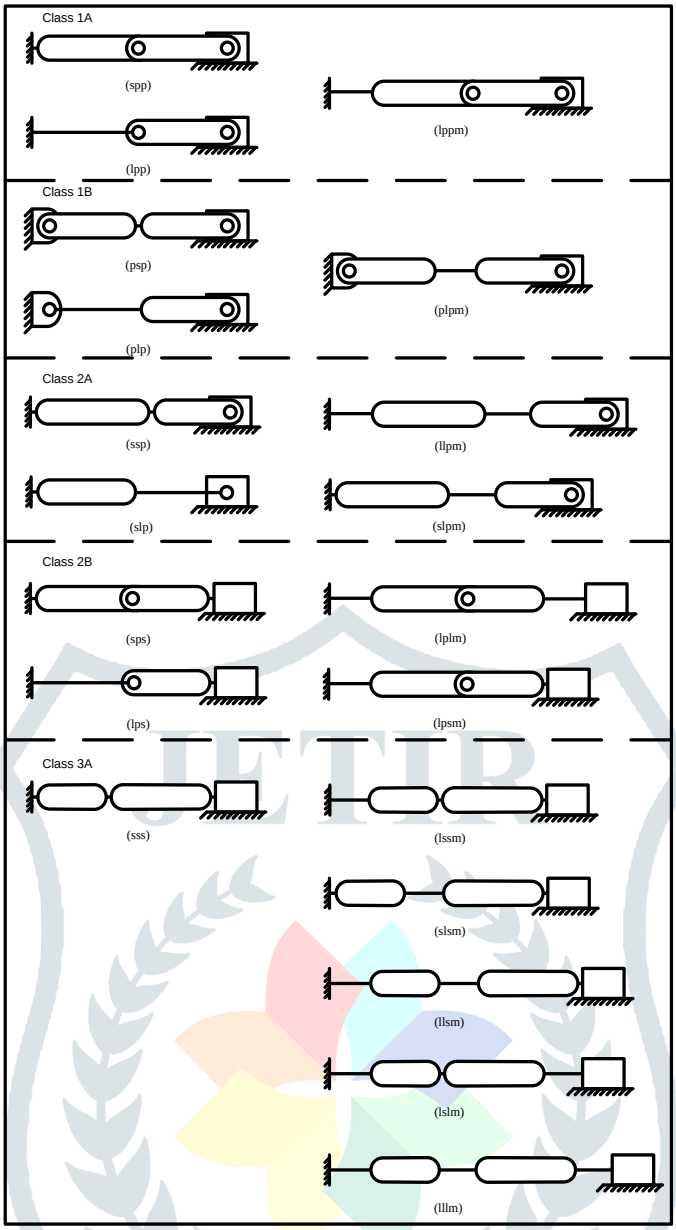

Fig. 1. Side-by-side comparison of the modified configurations of CFSMs with the original CFSMs

II. Description of the Modified CFSMs

As shown in Figure 1, Class 1A mechanisms are CFSMs that have one flexible segment located at the first pivot point, Class 1B are CFSMs that have one flexible segment located at the second pivot point, Class 2A mechanisms are CFSMs that have two flexible segments located at the first and second pivot points, Class 2B mechanisms are CFSMs that have two flexible segments located at the first and third pivot points, Class 3A mechanisms are CFSMs that have three flexible segments located at the first, second, and third pivot points. Each of the modified CFSMs shown in Fig. 1 is denoted by a string of letters representing the order and type of pivots used. The letters "s", "l", "p", and "m" represents short-length flexural pivot, long flexible beam, pin joint, and modified respectively [15].

III. The Generalized Pseudo-Rigid-Body Model (PRBM)

The generalized PRBM for all modified configurations of CFSMs presented in Figure 1 is shown in Figure 2; only half of the symmetric mechanism is shown [14; 15]. Each of the modified CFSMs presented in Figure 1 can be converted to its equivalent rigid-body counterpart by using the PRBM rule for small-length flexural pivots, the PRBM rule for modified long fixed-pinned flexible beams, the PRBM rule for modified long fixed-fixed flexible beams, or a combination of the PRBM rules as shown in Fig. 3, 4 and 5 [15]. The most straightforward alteration is that every flexible segment becomes two rigid segments joined by a pin and torsional spring. The generalized expression for the torsional spring constant k for the flexible segments is expressed as [14; 15; 16]

$$k = n\gamma K_\theta \frac{EI}{L} \quad (1)$$

Where γ is the PRBM characteristic radius factor, K_θ is a PRBM stiffness coefficient, E is the modulus of elasticity of material, I is the moment of inertia of the cross section of the flexible segment and L is the beam length. The average values for γ and K_θ over a wide range of loading conditions have been tabulated [6], but may be approximated for any material properties as 0.85 and 2.65 respectively for long flexible segments and for small-length flexural pivots, the values of γ and K_θ are 1. For long fixed-fixed flexible segments $n = 2$ and for long fixed-pinned flexible segments and short-length flexural pivots $n = 1$. Table 1 gives the x_b formulas for all modified configurations of CFSMs, Table 2 gives the spring constant formulas for all modified CFSMs.

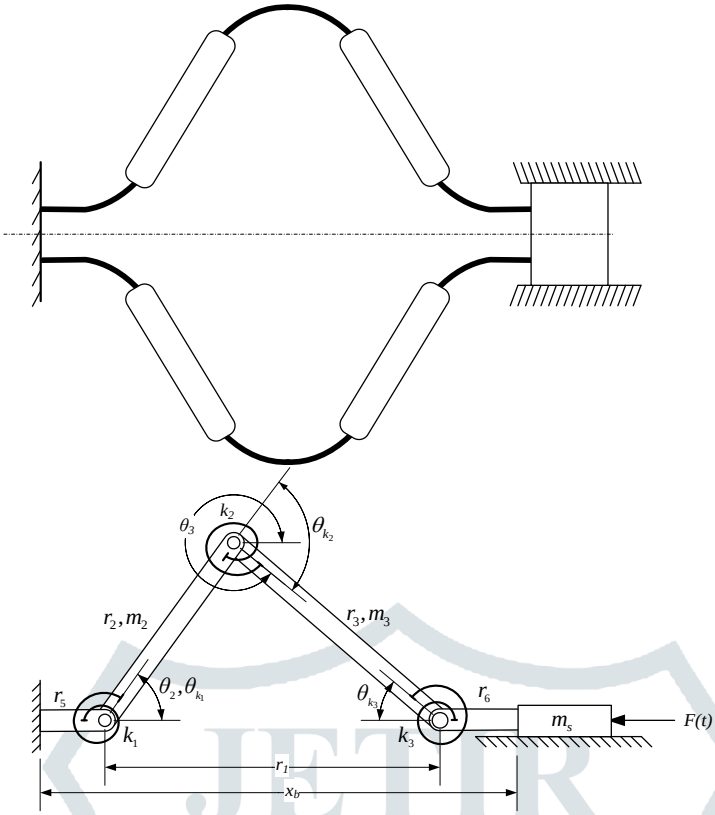

Fig. 2. Modified CFSM Class 3A-llm, and the generalized PRBM

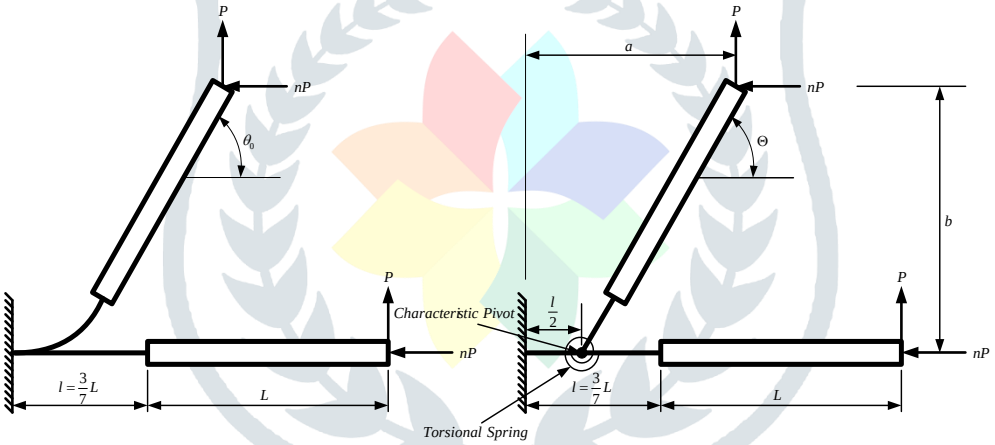

Fig. 3. Modified Cantilever Beam with Force at the End and its PRBM

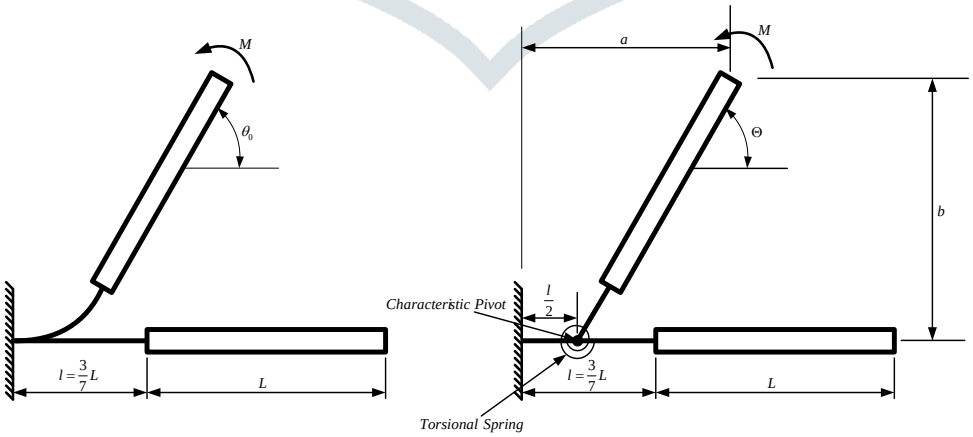

Fig. 4. Modified Cantilever Beam with End Moment Loading and its PRBM.

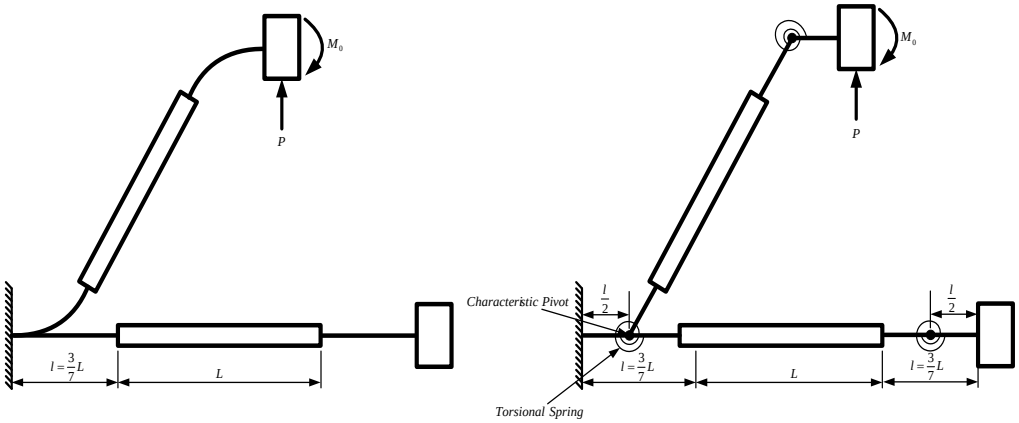

Fig. 5. Modified Fixed-Guided Beam and its PRBM

Table 1. x_b Formulas for the modified CFSMs

Modified CFSMs	x_b formula
Class 1A-lppm	$x_b = r_5 + r_1$
Class 1B-plpm	$x_b = r_1$
Class 2A-llpm	$x_b = r_5 + r_1$
Class 2A-slpm	$x_b = r_1$
Class 2B-lplm	$x_b = r_5 + r_1 + r_6$
Class 2B-lpsm	$x_b = r_5 + r_1$
Class 3A-lssm	$x_b = r_5 + r_1$
Class 3A-slsm	$x_b = r_1$
Class 3A-llsm	$x_b = r_5 + r_1$
Class 3A-lslm	$x_b = r_5 + r_1 + r_6$
Class 3A-lllm	$x_b = r_5 + r_1 + r_6$

Table 2. Spring Constant Formulas for the modified CFSMs

Modified CFSMs	k_1	k_2	k_3
Class 1A-lppm	$0.3\gamma K_\theta EI/L_1$	0	0
Class 1B-plpm	0	$0.3\gamma K_\theta EI/L_2$	0
Class 2A-llpm	$0.6\gamma K_\theta EI/L_1$	$0.3\gamma K_\theta EI/L_2$	0
Class 2A-slpm	EI/L_1	$0.3\gamma K_\theta EI/L_2$	0
Class 2B-lplm	$0.3\gamma K_\theta EI/L_1$	0	$0.3\gamma K_\theta EI/L_3$
Class 2B-lpsm	$0.3\gamma K_\theta EI/L_1$	0	EI/L_3
Class 3A-lssm	$0.3\gamma K_\theta EI/L_1$	EI/L_2	EI/L_3
Class 3A-slsm	EI/L_1	$0.3\gamma K_\theta EI/L_2$	EI/L_3
Class 3A-llsm	$0.6\gamma K_\theta EI/L_1$	$0.3\gamma K_\theta EI/L_2$	EI/L_3
Class 3A-lslm	$0.3\gamma K_\theta EI/L_1$	EI/L_2	$0.3\gamma K_\theta EI/L_3$
Class 3A-lllm	$0.6\gamma K_\theta EI/L_1$	$0.6\gamma K_\theta EI/L_2$	$0.6\gamma K_\theta EI/L_3$

Fig. 6 gives the definition of flexible and rigid segment lengths, Table 3 gives the flexible and rigid segment lengths for all modified configurations of CFSMs and Table 4 gives the length parameter formulas and values for all modified configurations of CFSMs. The following expressions, along with the definition in Figure 6, together with those tabulated in Table 3, may be used to determine the length of the flexible and rigid segments for all modified configurations of CFSMs [15].

$r_{Tot} = r_2 + r_3 =$ Total PRBM length (2)

$r_2 = \frac{r_{Tot}}{(R+1)}$ (3)

$r_3 = \frac{r_{Tot}}{\left(\frac{1}{R}+1\right)}$ (4)

$R = \frac{r_3}{2_2} =$ Geometric parameter ratio (5)

$\Lambda = \frac{L_{Tot}}{r_{Tot}} =$ Length parameter ratio (6)

$L_{Tot} =$ Total length of actual modified CFSMs

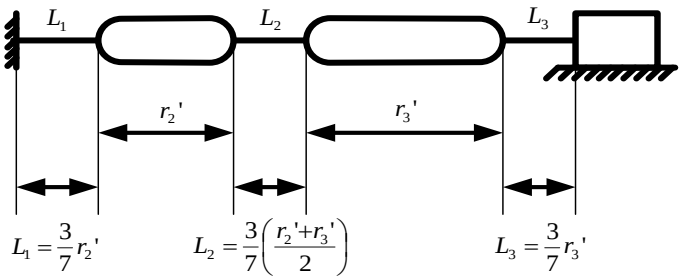

Fig. 6. Definition of CFSMs flexible and rigid segment lengths

Table 3. Flexible and rigid segment lengths for the modified CFSMs

To get:	L_1	L_2	L_3	r_2'	r_3'
Modified CFSMs	Multiply r_2' by	Multiply r_{ave}' by	Multiply r_3' by	Subtract from r_2	Subtract from r_3

Class 1A-lppm	3/7	0	0	$0.5 \times L_1$	0
Class 1B-plpm	0	3/7	0	$0.5 \times L_2$	$0.5 \times L_2$
Class 2A-llpm	3/7	3/7	0	$0.5 \times (L_1 + L_2)$	$0.5 \times L_2$
Class 2A-slpm	0.1	3/7	0	$0.5 \times (L_1 + L_2)$	$0.5 \times L_2$
Class 2B-lplm	3/7	0	3/7	$0.5 \times L_1$	$0.5 \times L_3$
Class 2B-lpsm	3/7	0	0.1	$0.5 \times L_1$	$0.5 \times L_3$
Class 3A-lssm	3/7	0.1	0.1	$0.5 \times (L_1 + L_2)$	$0.5 \times (L_2 + L_3)$
Class 3A-slsm	0.1	3/7	0.1	$0.5 \times (L_1 + L_2)$	$0.5 \times (L_2 + L_3)$
Class 3A-llsm	3/7	3/7	0.1	$0.5 \times (L_1 + L_2)$	$0.5 \times (L_2 + L_3)$
Class 3A-lslm	3/7	0.1	3/7	$0.5 \times (L_1 + L_2)$	$0.5 \times (L_2 + L_3)$
Class 3A-lllm	3/7	3/7	3/7	$0.5 \times (L_1 + L_2)$	$0.5 \times (L_2 + L_3)$

Table 4. Length Parameter Formulas and Values for the modified CFSMs

Modified CFSMs	Length parameter ʎ formula	ʎ values	R values
Class 1A-lppm	$(R\gamma + 1)/\gamma(R + 1)$	1.0882	1.0000
Class 1B-plpm	$(R + 1)/(R + 1)$	1.0000	0.9000
Class 2A-llpm	$(0.7R + \gamma)/\gamma^2(R + 1)$	1.0677	1.1000
Class 2A-slpm	$(R + 1.05)/(R + 1)$	1.0238	1.1000
Class 2B-lplm	$(R + 1)/\gamma(R + 1)$	1.1765	1.0000
Class 2B-lpsm	$(1.05R\gamma + 1)/\gamma(R + 1)$	1.1102	1.1000
Class 3A-lssm	$(0.89R + 1)/\gamma(R + 1)$	1.1071	1.0000
Class 3A-slsm	$(1.04R + 1.04)/(R + 1)$	1.0400	1.0000
Class 3A-llsm	$(0.99R + 0.87)/\gamma(R + 1)$	1.0941	1.0000
Class 3A-lslm	$(0.99R + 0.99)/\gamma(R + 1)$	1.1694	1.0000
Class 3A-lllm	$(1.15R + 1.15)/(R + 1)$	1.1500	1.0000

IV. LAGRANGE'S EQUATIONS FORMULATION FOR THE GENERALIZED PRBM

With the generalized PRBM clearly defined as shown in Fig. 2, the generalized equation of motion for all modified CFSMs configurations may be obtained using Lagrange's method. Taking θ_2 as the generalized position coordinate and neglecting the effect of damping on the modified CFSM model, Lagrange's equation for a dynamic system may be expressed as [12]

$$\frac{d}{dt}\left(\frac{\delta(T-V)}{\delta\dot{\theta}_2}\right) - \frac{\delta(T-V)}{\delta\theta_2} = Q_{\theta 2} \quad (7)$$

$Q_{\theta 2}$ is the generalized force which can either be a force or a moment derivable from the corresponding work done by the respective agent. The total potential energy in the mechanism assuming negligible potential energy due to gravity is the sum of the individual potential energy stored in each compliant segment. For the modified CFSM model, the generalized potential energy equation is given as [15]

$$V = \frac{1}{2}(k_1\theta_{k1}^2 + k_2\theta_{k2}^2 + k_3\theta_{k3}^2) \quad (8)$$

Where k_1, k_2, and k_3 are the torsional spring constants and θ_{k1}, θ_{k2}, and θ_{k3} are the relative deflections of the torsional springs which may be obtained from the following expressions

$$\theta_{k1} = \theta_2 \quad (9)$$

$$\theta_{k2} = \theta_2 + \theta_{k3} \quad (10)$$

$$\theta_{k3} = \sin^{-1}\left(\frac{r_2}{r_3}\sin\theta_2\right) \quad (11)$$

Substituting equations (9), (10), and (11) into equation (8), the expression for the potential energy therefore becomes

$$V = \frac{1}{2}\left(k_1\theta_2^2 + k_2\left(\theta_2 + \sin^{-1}\left(\frac{r_2}{r_3}\sin\theta_2\right)\right)^2 + k_3\left(\sin^{-1}\left(\frac{r_2}{r_3}\sin\theta_2\right)\right)^2\right) \quad (12)$$

For the modified CFSM model, the generalized kinetic energy equation is given as [15]

$$T = \frac{1}{2}m_2V_{C2}^2 + \frac{1}{2}m_3V_{C3}^2 + \frac{1}{2}m_S\dot{r}_1^2 + \frac{1}{2}J_{C2}\dot{\theta}_2^2 + \frac{1}{2}J_{C3}\dot{\theta}_3^2 \quad (13)$$

Where m_1 and m_2 are the mass of links 2 and 3, V_{C1} and V_{C2} are the velocity of the center of mass of links 2 and 3, J_{C2} and J_{C3} are the mass moment of inertia of links 2 and 3 about the center of mass, $\dot{\theta}_2$ and $\dot{\theta}_3$ are the angular velocity of links 2 and 3, m_S is the mass of the slider, and $\dot{r}_1$ is the velocity of the slider. The first three terms of the kinetic energy expression represent the translational energy of the system, and the last two represent the rotational energy.

$$V_{C2} = \frac{1}{2}r_2\dot{\theta}_2 \quad (14)$$

$$V_{C2}^2 = \frac{1}{4}r_2^2\dot{\theta}_2^2 \quad (15)$$

$$V_{C3} = \left(r_2^2\dot{\theta}_2^2 + r_2r_3\cos(\theta_2 - \theta_3)\dot{\theta}_2\dot{\theta}_3 + \frac{1}{4}r_3^2\dot{\theta}_3^2\right)^{\frac{1}{2}} \quad (16)$$

$$V_{C3}^2 = r_2^2\dot{\theta}_2^2 + r_2r_3\cos(\theta_2 - \theta_3)\dot{\theta}_2\dot{\theta}_3 + \frac{1}{4}r_3^2\dot{\theta}_3^2 \quad (17)$$

$$V_{C3}^2 = r_2^2\sin^2\theta_2\dot{\theta}_2^2 + \left(\frac{1}{4}\right)\frac{r_2^2r_3^2\cos^2\theta_2}{r_3^2 - r_2^2\sin^2\theta_2}\dot{\theta}_2^2 + \frac{r_2^3\sin^2\theta_2\cos\theta_2}{\sqrt{r_3^2 - r_2^2\sin^2\theta_2}}\dot{\theta}_2^2 \quad (18)$$

$$\dot{r}_1 = -r_2\sin\theta_2\dot{\theta}_2 - r_3\sin\theta_3\dot{\theta}_3 \quad (19)$$

$$\dot{r}_1^2 = r_2^2\sin^2\theta_2\dot{\theta}_2^2 + 2r_2r_3\sin\theta_2\sin\theta_3\dot{\theta}_2\dot{\theta}_3 + r_3^2\sin^2\theta_3\dot{\theta}_3^2 \quad (20)$$

$$\dot{r}_1^2 = r_2^2\sin^2\theta_2\dot{\theta}_2^2 + \frac{r_2^4\sin^2\theta_2\cos^2\theta_2}{r_3^2 - r_2^2\sin^2\theta_2}\dot{\theta}_2^2 + \frac{2r_2^3\sin^2\theta_2\cos\theta_2}{\sqrt{r_3^2 - r_2^2\sin^2\theta_2}}\dot{\theta}_2^2 \quad (21)$$

$$\dot{\theta}_3 = -\frac{r_2\cos\theta_2}{r_3\cos\theta_3}\dot{\theta}_2 \quad (22)$$

$$\dot{\theta}_3^2 = \frac{r_2^2\cos^2\theta_2}{r_3^2\cos^2\theta_3}\dot{\theta}_2^2 \quad (23)$$

$$\dot{\theta}_3^2 = \frac{r_2^4\cos^2\theta_2}{r_3^2 - r_2^2\sin^2\theta_2}\dot{\theta}_2^2 \quad (24)$$

Substituting equations (15), (18), (21), and (24) into equation (13) the expression for the kinetic energy therefore becomes

$$T = \left[m_2\left(\frac{1}{6}r_2^2\right) + m_3\left(\frac{1}{2}\frac{r_3^3\sin^2\theta_2\cos\theta_2}{\sqrt{r_3^2 - r_2^2\sin^2\theta_2}} + \frac{1}{6}\frac{r_2^2 r_3^2\cos^2\theta_2}{r_3^2 - r_2^2\sin^2\theta_2} + \frac{1}{2}r_2^2\sin^2\theta_2\right) + m_S\left(\frac{r_3^2\sin^2\theta_2\cos\theta_2}{\sqrt{r_3^2 - r_2^2\sin^2\theta_2}} + \frac{1}{2}\frac{r_2^4\sin^2\theta_2\cos^2\theta_2}{r_3^2 - r_2^2\sin^2\theta_2} + \frac{1}{2}r_2^2\sin^2\theta_2\right)\right]\dot{\theta}_2^2 \quad (25)$$

The generalized forcing function $Q_{\theta 2}$ consists of a moment τ_F due directly to the force F acting on the slider and the terms τ_{CF} and τ_{AF} are introduced to compensate for the moment due to Coulomb pin friction and that due to axial force effects in the mechanism's pin joints, and links/segments of the modified CFSMs respectively [15]. Because the modified CFSM Class 3A-lllm contains no rigid joints, its operation is friction-free, with no backlash or wear [14; 15]. In mathematical terms, the generalized forcing function $Q_{\theta 2}$ is given by the following expression

$$Q_{\theta 2} = \frac{d}{dt}\left(\frac{\delta(T-V)}{\delta\dot{\theta}_2}\right) - \frac{\delta(T-V)}{\delta\theta_2} = \tau_F + \tau_{CF} + \tau_{AF} \quad (26)$$

The generalized expression for the moment due to Coulomb pin friction τ_{CF} is given as [15]

$$\tau_{CF} = \left(C_1\theta_2 + C_2\theta_2\left(1 + \frac{r_2\cos\theta_2}{\sqrt{r_3^2 - r_2^2\sin^2\theta_2}}\right) + C_3\theta_2\left(\frac{r_2\cos\theta_2}{\sqrt{r_3^2 - r_2^2\sin^2\theta_2}}\right)\right)\text{sign}(\dot{\theta}_2) \quad (27)$$

Where $C_1, C_2, and\ C_3$ are the coulomb friction coefficients at the different pivot points which are usually obtained from experimentation. The value of the torque τ_{AF} may be approximated using the expression given below

$$\tau_{AF} = F_{static}r_2\alpha\left(1 + \frac{r_2}{\sqrt{r_3^2 - r_2^2\alpha^2}}\right) \propto \text{is the angle of axial force effect} \quad (28)$$

Note that because θ_2 is an angle, the generalized forcing function $Q_{\theta 2}$ has the dimension of moment. τ_F may therefore be transformed to the mechanism's output force F using the power relationship as follows:

$$F\dot{r}_1 = F\dot{\theta}_2\left(-r_2\sin\theta_2 - \frac{r_2^2\sin\theta_2\cos\theta_2}{\sqrt{r_3^2 - r_2^2\sin^2\theta_2}}\right) = \tau_F\dot{\theta}_2 = \left(\left(\frac{d}{dt}\left(\frac{\delta(T-V)}{\delta\dot{\theta}_2}\right) - \frac{\delta(T-V)}{\delta\theta_2}\right) - \tau_{CF} - \tau_{AF}\right)\dot{\theta}_2 \quad (29)$$

Substituting equations (12), (25), (27), and (28) into equation (29) and simplifying, gives the Generalized Mathematical Dynamic Model (GMDM) for all modified configurations of CFSMs

$$\begin{aligned} F \times \left(-r_2\sin\theta_2 - \frac{r_2^2\sin\theta_2\cos\theta_2}{\sqrt{r_3^2 - r_2^2\sin^2\theta_2}}\right) &= \left[m_2\left(\frac{1}{3}r_2^2\right) + m_3\left(\frac{r_3^3\sin^2\theta_2\cos\theta_2}{\sqrt{r_3^2 - r_2^2\sin^2\theta_2}} + \frac{1}{3}\frac{r_2^2 r_3^2\cos^2\theta_2}{r_3^2 - r_2^2\sin^2\theta_2} + r_2^2\sin^2\theta_2\right)\right. \\ &\left. + m_S\left(\frac{r_2^4\sin^2\theta_2\cos^2\theta_2}{r_3^2 - r_2^2\sin^2\theta_2} + \frac{2r_3^3\sin^2\theta_2\cos\theta_2}{\sqrt{r_3^2 - r_2^2\sin^2\theta_2}} + r_2^2\sin^2\theta_2\right)\right]\ddot{\theta}_2 \\ &+ \left[m_3\left(\frac{1}{2}\frac{r_2^5\sin^3\theta_2\cos^2\theta_2}{(r_3^2 - r_2^2\sin^2\theta_2)^{\frac{3}{2}}} + \frac{1}{3}\frac{r_2^4 r_3^2\sin\theta\cos^3\theta_2}{(r_3^2 - r_2^2\sin^2\theta_2)^2} - \frac{1}{2}\frac{r_2^3\sin^3\theta_2}{\sqrt{r_3^2 - r_2^2\sin^2\theta_2}} + \frac{r_2^3\sin\theta\cos^2\theta_2}{\sqrt{r_3^2 - r_2^2\sin^2\theta_2}} - \frac{1}{3}\frac{r_2^2 r_3^2\sin\theta_2\cos\theta_2}{r_3^2 - r_2^2\sin^2\theta_2}\right. \\ &\left. + r_2^2\sin\theta_2\cos\theta_2\right) \\ &+ m_S\left(\frac{r_2^6\sin^3\theta_2\cos^3\theta_2}{(r_3^2 - r_2^2\sin^2\theta_2)^2} + \frac{r_2^5\sin^3\theta_2\cos^2\theta_2}{(r_3^2 - r_2^2\sin^2\theta_2)^{\frac{3}{2}}} - \frac{r_2^4\sin^3\theta_2\cos\theta_2}{r_3^2 - r_2^2\sin^2\theta_2} + \frac{r_2^4\sin\theta_2\cos^3\theta_2}{r_3^2 - r_2^2\sin^2\theta_2} + \frac{2r_3^2\sin\theta_2\cos^2\theta_2}{\sqrt{r_3^2 - r_2^2\sin^2\theta_2}}\right. \\ &\left. - \frac{r_2^3\sin^3\theta_2}{\sqrt{r_3^2 - r_2^2\sin^2\theta_2}} + r_2^2\sin\theta_2\cos\theta_2\right)\Big]\dot{\theta}_2^2 + k_1\theta_2 + k_2\left(\theta_2 + \sin^{-1}\left(\frac{r_2}{r_3}\sin\theta_2\right)\right)\left(1 + \frac{r_2\cos\theta_2}{\sqrt{r_3^2 - r_2^2\sin^2\theta_2}}\right) \\ &+ k_3\left(\sin^{-1}\left(\frac{r_2}{r_3}\sin\theta_2\right)\right)\left(\frac{r_2\cos\theta_2}{\sqrt{r_3^2 - r_2^2\sin^2\theta_2}}\right) \\ &- \left(C_1\theta_2 + C_2\theta_2\left(1 + \frac{r_2\cos\theta_2}{\sqrt{r_3^2 - r_2^2\sin^2\theta_2}}\right) + C_3\theta_2\left(\frac{r_2\cos\theta_2}{\sqrt{r_3^2 - r_2^2\sin^2\theta_2}}\right)\right)\text{sign}(\dot{\theta}_2) - F_{static}r_2\alpha\left(1 + \frac{r_2}{\sqrt{r_3^2 - r_2^2\alpha^2}}\right) \end{aligned} \quad (30)$$

V. Experimentation and Discussion of Results

Table 5 gives the parameters and values for all modified configurations of CFSMs. Table 6 gives the extended length, fully compressed mechanism length, nominal constant force, and average non-dimensionalized constant for a 40% slider displacement for all modified configurations of CFSMs. Fig. 7 shows the schematic of a special multi-purpose experimental setup that was designed to test the validity of both the static and dynamic models [15]. The setup was designed to allow the testing of the modified CFSMs by sinusoidally cycling them through compression and expansion at different frequencies. The modified CFSMs as shown in Fig. 7 are bolted to a thick steel ground mounted perpendicular to a steel table. In this manner, both ground pivots of the modified CFSMs are fixed with respect to the table. The modified CFSMs slider is actuated by a steel block free to move across a linear bearing. Driving the actuator block is a velocity-controlled 1hp motor with a rotor and crank arm. The center of the motor shaft and the point of attachment of the crank arm to the actuator block share the same height as the base table. Assuming a constant angular velocity of the motor and a small crank radius r, the actuator block drives the modified CFSMs with an

approximately sinusoidal velocity. The rotor is drilled with a series of tapped holes each located at a different radius for variable positioning of the crank arm. This allows for larger or smaller total linear displacements of the modified CFSMs as the rotor cycles. Bolted in-line between the actuator block and modified CFSMs is a load cell that measures the force exerted on the slider. The load cell used is a Compression Digital USB Load Cell with digital perfection for load and force measurement, with an accuracy of 0.050%. It offers direct measurement of loads via the USB port of a PC, it does not require signal conditioners, data acquisition systems, or special software. The power supply is via a USB port with integrated power conditioning. It is mechanically robust, rugged, and has a compact design with a low profile and stainless steel construction. It also has a threaded mounting hole for easy attachment using standard fixtures.

Table 5. Parameters and Values for all modified configurations of CFSMs

Parameter	Class 1A-lppm	Class 1B-plpm	Class 2A-llpm	Class 2B-lplm	Class 3A-lssm
r_2	73.5135 mm	84.2105 mm	71.3580 mm	68.0000 mm	72.2635 mm
r_3	73.5135 mm	75.7895 mm	78.4938 mm	68.0000 mm	72.2635 mm
r_5	12.9730 mm	-	10.4215 mm	12.0000 mm	12.2103 mm
r_6	-	-	-	12.0000 mm	-
m_2	76.1446 g	78.3494 g	97.1555 g	74.1147 g	100.5655 g
m_3	51.8910 g	75.3607 g	76.5531 g	74.1147 g	101.2889 g
m_S	75.7979 g	75.7979 g	75.7979 g	116.7138 g	116.7138 g
b	25.40 mm	25.40 mm	25.40 mm	25.40 mm	25.40 mm
h_1	0.5602 mm	-	0.2102 mm	0.5181 mm	0.5272 mm
h_2	-	0.3042 mm	0.2652 mm	-	0.0448 mm
h_3	-	-	-	0.5181 mm	0.0961 mm
E	207 Gpa	207 Gpa	207 Gpa	207 Gpa	207 Gpa
l_1	25.9459 mm	-	20.8431 mm	24.0000 mm	24.4206 mm
l_2	-	28.2353 mm	24.6054 mm	-	6.1439 mm
l_3	-	-	-	24.0000 mm	6.5897 mm
k_1	4.0113 Nm	-	0.5279 Nm	3.4322 Nm	3.5535 Nm
k_2	-	0.5903 Nm	0.4487 Nm	-	0.0128 Nm
k_3	-	-	-	3.4322 Nm	0.1182 Nm
Parameter	Class 3A-slsm	Class 3A-llsm	Class 3A-lslm	Class 3A-lllm	Class 3A-lllRig
r_2	76.9231 mm	73.1183 mm	68.4105 mm	69.5652 mm	69.5652 mm
r_3	76.9231 mm	73.1183 mm	68.4105 mm	69.5652 mm	69.5652 mm
r_5	-	10.8405 mm	11.5950 mm	10.4348 mm	10.1098 mm
r_6	-	-	11.5950 mm	10.4348 mm	10.1098 mm
m_2	100.8852 g	97.8628 g	99.2904 g	96.4089 g	3.6762 g
m_3	100.8852 g	99.7599 g	99.2904 g	96.4089 g	57.4004 g
m_S	116.7138 g	116.7138 g	116.7138 g	116.7138 g	118.1804 g
b	25.40 mm	25.40 mm	25.40 mm	25.40 mm	25.4000 mm
h_1	0.0888 mm	0.2340 mm	0.5007 mm	0.2253 mm	0.1325 mm
h_2	0.2815 mm	0.2523 mm	0.0395 mm	0.1126 mm	0.1325 mm
h_3	0.0888 mm	0.0854 mm	0.5007 mm	0.2253 mm	0.2183 mm
E	207 Gpa	207 Gpa	207 Gpa	207 Gpa	207 Gpa
l_1	6.0843 mm	21.6811 mm	23.1900 mm	20.8696 mm	67.3988 mm
l_2	26.0756 mm	23.3772 mm	5.4110 mm	20.8696 mm	81.8414 mm
l_3	6.0843 mm	5.8504 mm	23.1900 mm	20.8696 mm	20.2196 mm
k_1	0.1007 Nm	0.7002 Nm	3.2044 Nm	0.6488 Nm	0.1363 Nm
k_2	0.5064 Nm	0.4070 Nm	0.0100 Nm	0.0811 Nm	0.1123 Nm
k_3	0.1007 Nm	0.0931 Nm	3.2044 Nm	0.6488 Nm	0.6090 Nm

Table 6. Extended Length, Fully Compressed Mechanism Length, Nominal Constant Force, and Average Non-Dimensionalized Constant for a 40% Slider Displacement for all Modified configurations of CFSMs

Parameter	Class 1A-lppm	Class 1B-plpm	Class 2A-llpm
x_b max	160.0000 mm	160.0000 mm	160.0000 mm
x_b min	101.1892 mm	96.0000 mm	100.3326 mm
F_{Nom}	59.0781 N	32.0878 N	34.8222 N
ϕ	0.5413	2.2889	2.3533
Parameter	Class 2B-lplm	Class 3A-lssm	Class 3A-slsm
x_b max	160.0000 mm	156.7374 mm	153.8462 mm
x_b min	105.6000 mm	98.9265 mm	92.3077 mm
F_{Nom}	109.2944 N	55.7807 N	31.3481 N
ϕ	1.0827	0.5672	2.3807
Parameter	Class 3A-llsm	Class 3A-lslm	Class 3A-lllm
x_b max	157.0771 mm	160.0000 mm	160.0000 mm
x_b min	98.5825 mm	105.2825 mm	104.3478 mm
F_{Nom}	35.8571 N	102.0596 N	25.2446 N

ϕ	1.8721	1.0894	1.3534

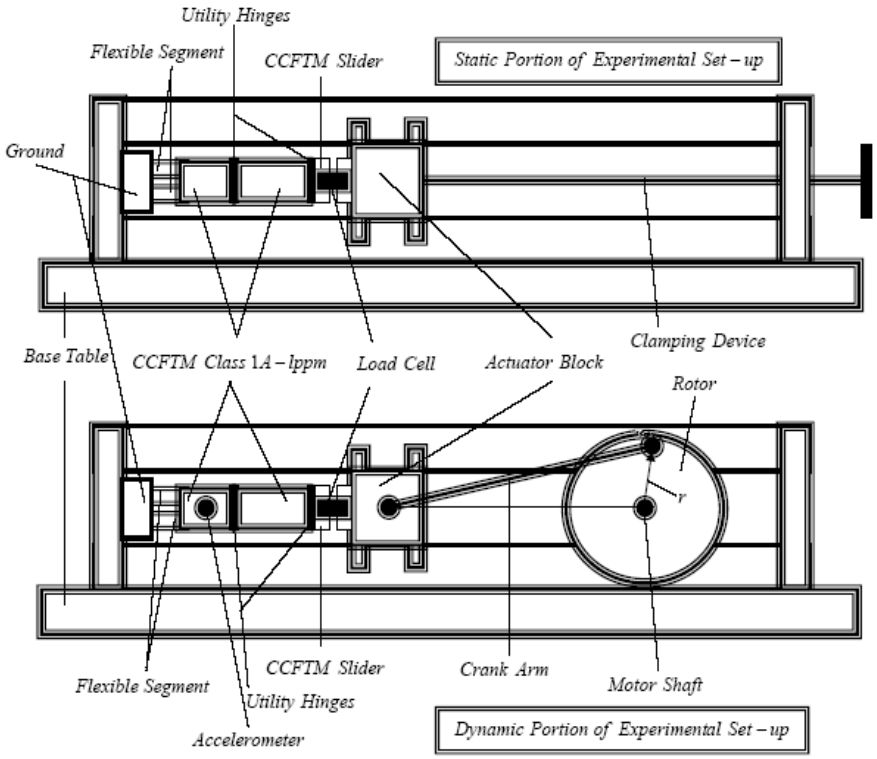

Fig. 7. Schematic of the Multi-purpose Experimental Set-up

In the dynamic evaluation of all modified configurations of CFSMs, three useful plots were analyzed, the mean force plot, the median force plot and the peak-to-peak force magnitude difference plot as a function of frequency for a 40% slider displacement as shown in Fig. 8, 9 and 10 for the modified CFSM Class 2B-lplm. Each frequency assumes a sinusoidal position input with amplitude equal to the full 40% designed mechanism deflection with a slight pre-displacement to give a preload at full expansion. The first curve in each of the figures represents the force predicted by the dynamic model with all parameters as defined in Table 5. The second and third curves are purely theoretical; what happens when the mass of the modified CFSMs slider is set to zero, or the modified CFSMs has no inertia at all (all masses set to zero). Setting all inertias to zero provides a baseline useful for comparison of the other curves and setting the end mass to zero shows the dynamic response of the modified CFSMs isolated as a separate module. The forth curve shows the result of experiment. Notice that each curve in the peak-to-peak force plot first curves down, then sustains a linear range before it starts to increase (all except for the third curve). This dip in magnitude difference is demonstrated clearly in Fig. 11, 12 and 13. As shown in the figures, the force profile at $\omega = 31.416$rad/s has a lower peak-to-peak force difference than the profiles at $\omega = 10.472$rad/s and $\omega = 62.832$rad/s. This very interesting phenomenon of the peak-to-peak force plot shows the range of frequencies over which the modified configurations of CFSMs exhibits better constant-force behavior than they do statically. In fact, the same observation was made by Boyle [1], Ugwuoke [13], Ugwuoke, Abolarin and Ogwuagwu [14], and Ugwuoke [15] while studying the dynamics of CFSMs. The knowledge of such a phenomenon makes modified CFSMs much more attractive for application in dynamic systems. This range of frequencies can be maximized by minimizing the slider mass as much as possible, this is clearly demonstrated by the second curve. This better constant-force behavior is likely due to inertial effects as evidenced by the third curve which represents the dynamic model with all of the inertias set to zero, which exhibits no dip in peak-to-peak force. Depending on what attributes are most desirable; a wide frequency band with moderately low peak-to-peak force, a single frequency with very low peak-to-peak force, or some other similar effects, the modified CFSMs parameters can be optimized to achieve the desired results [15]. The test result as demonstrated by the forth curve shows that the model actually predicted the performance of the modified CFSMs prototype. The modeled force does not match the measured force point for point, but predicted the mean force, median force, peak-to-peak force difference and the general shape of the force profile at any given frequency.

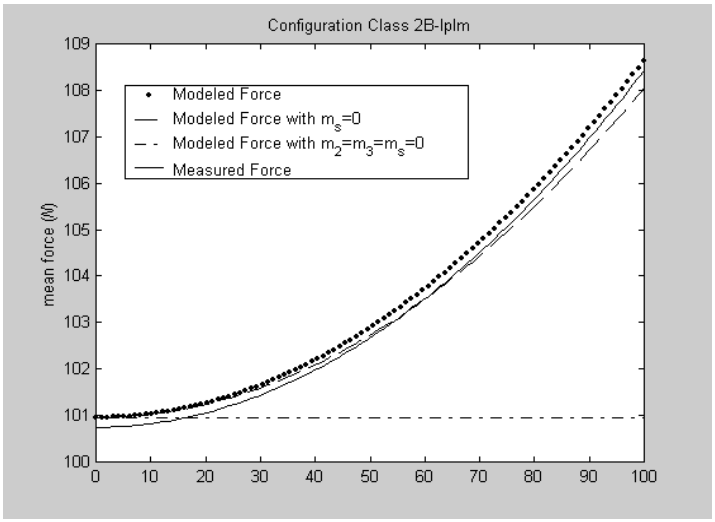

Fig. 8. The Mean Force as a Function of Frequency for the Modified CFSM Class 2B-lplm

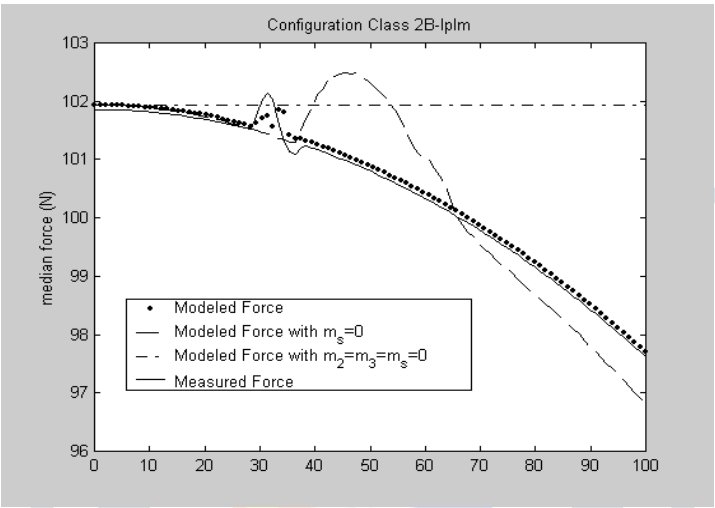

Fig. 9. The Median Force as a Function of Frequency for the Modified CFSM Class 2B-lplm

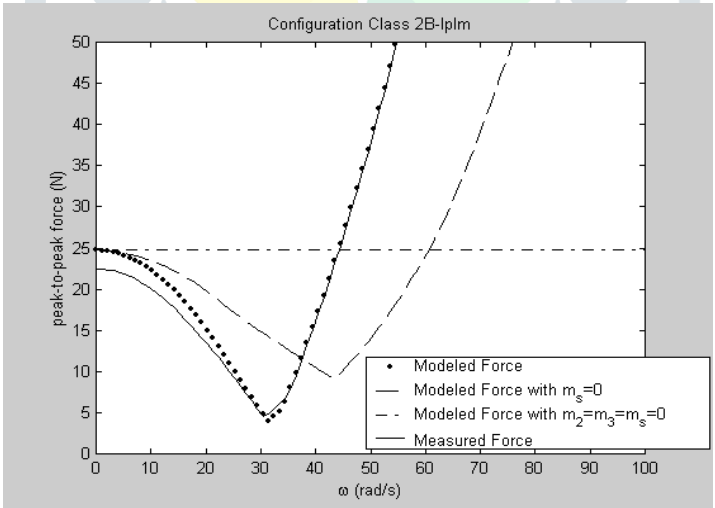

Fig. 10. The Peak-to-Peak Force Difference as a Function of Frequency for the Modified CFSM Class 2B-lplm

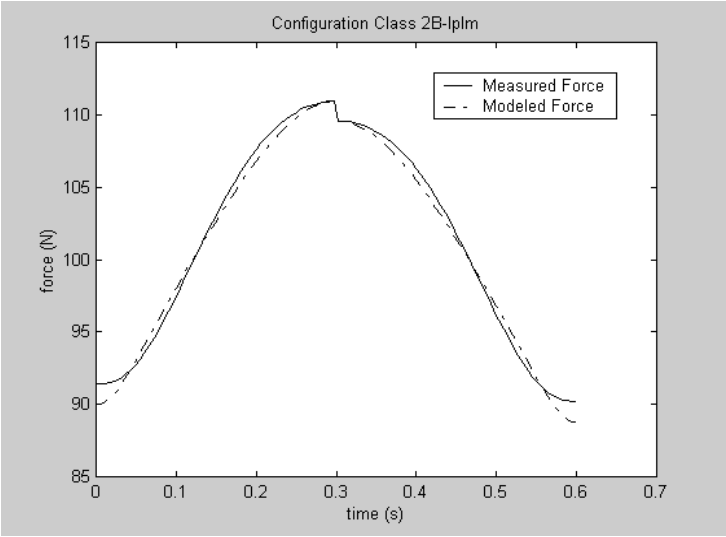

Fig. 11. Plot of Measured Force and Force Predicted by the Dynamic Model for $\omega = 10.472$ rad/s (Class 2B-lplm)

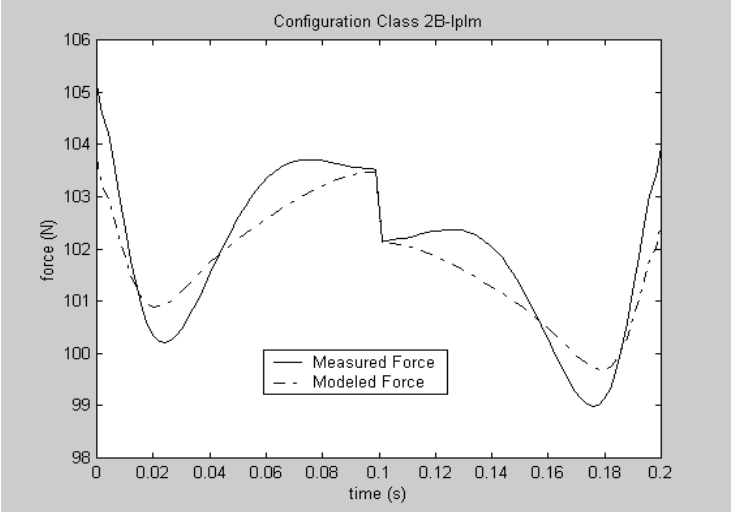

Fig. 12. Plot of Measured Force and Force Predicted by the Dynamic Model for $\omega = 31.416$ rad/s (Class 2B-lplm)

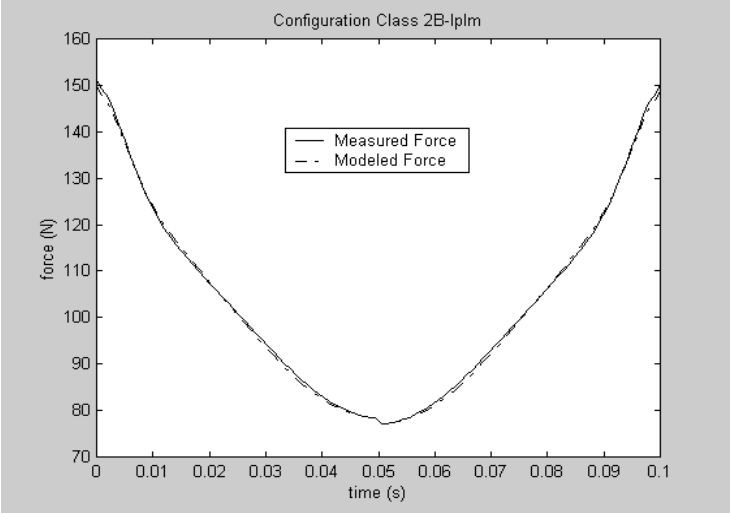

Fig. 13. Plot of Measured Force and Force Predicted by the Dynamic Model for $\omega = 62.832$ rad/s (Class 2B-lplm)

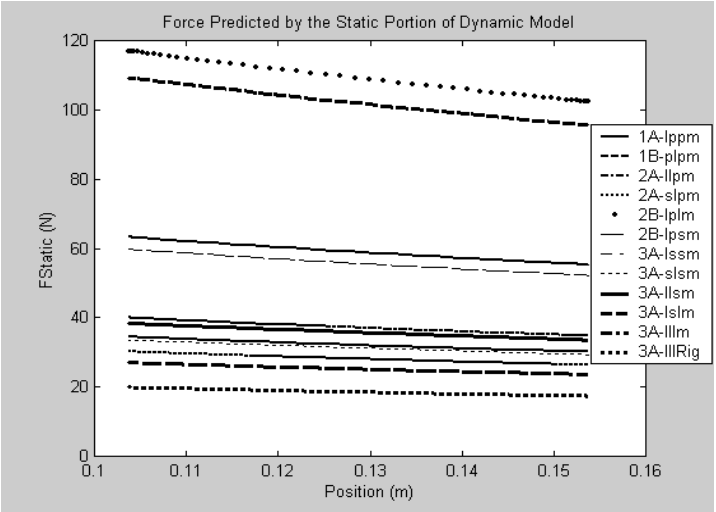

Fig. 14. Force Displacement Plot Showing the Force Predicted by the Static Portion of the Dynamic Model for a 40% Slider Displacement for all Modified Configurations of CFSMs

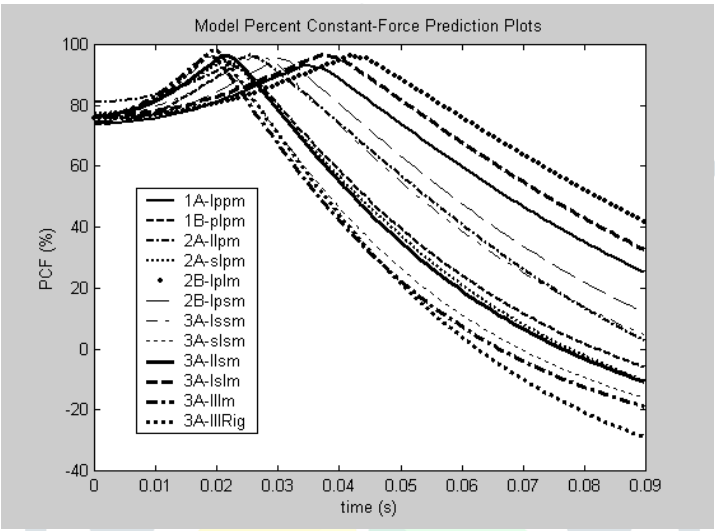

Fig. 15. Percent Constant-Force Prediction Plot as a Function of Time for a 40% Slider Displacement for all Modified Configurations of CFSMs

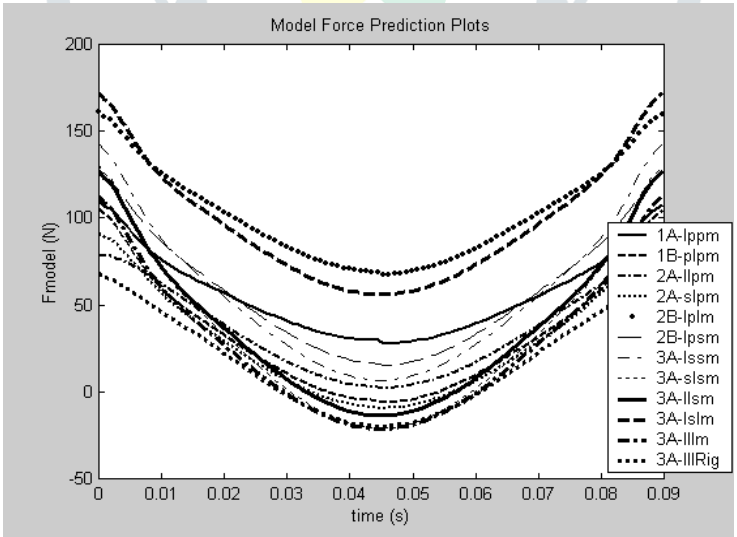

Fig. 16. Model Force Prediction Plot as a Function of Time for a 40% Slider Displacement for all Modified Configurations of CFSMs

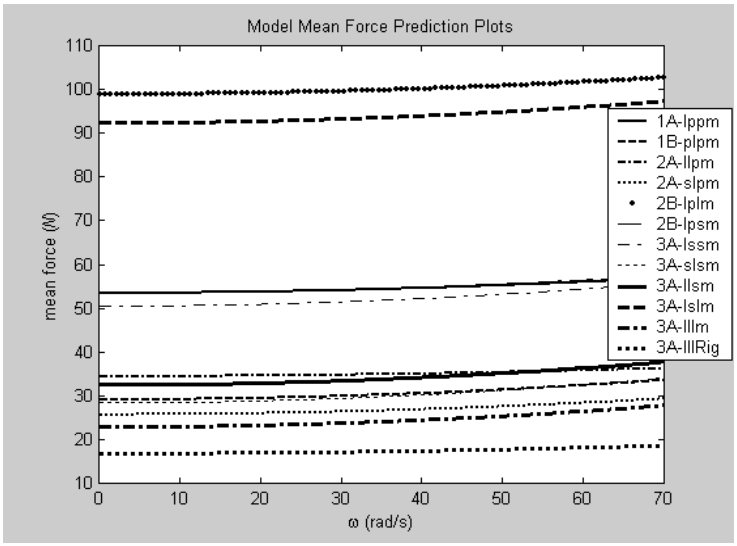

Fig. 17. Mean Force Plot as a Function of Frequency for a 40% Slider Displacement for all Modified Configurations of CFSMs

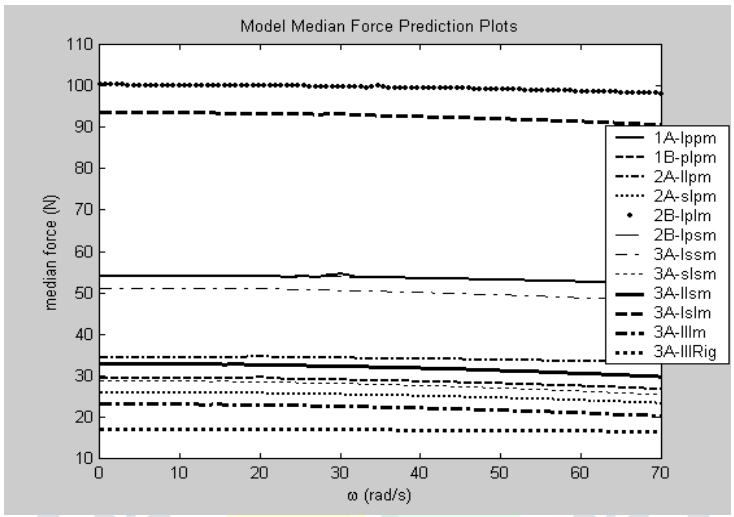

Fig. 18. Median Force Plot as a Function of Frequency for a 40% Slider Displacement for all Modified Configurations of CFSMs

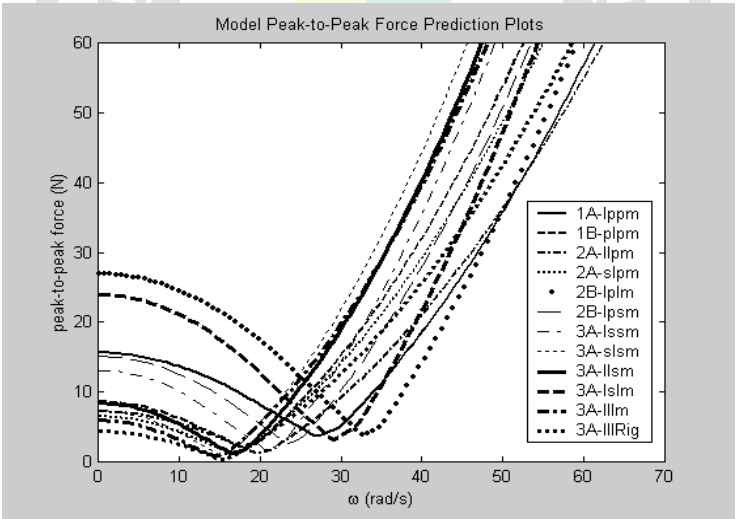

Fig. 19. Peak-to-Peak Force Plot as a Function of Frequency for a 40% Slider Displacement for all Modified Configurations of CFSMs

Table 10. Summary of Results for a Single Frequency with Very Low Peak-to-Peak Force for all Modified Configurations of CFSMs

Modified Configurations	Frequency (rad/s)	STDev Static	STDev Dynamic	Mean Force (N)	Median Force (N)	PCF (%)

		(N)	(N)			
Class 1A-lppm	27.0	±2.8314	±0.4849	53.8360	53.8383	96.7608
Class 1B-plpm	18.0	±1.5709	±0.2980	29.2195	29.1910	96.0560
Class 2A-llpm	20.0	±2.2243	±0.2220	33.3436	33.3316	97.6333
Class 2A-slpm	23.0	±2.6734	±0.1752	50.8339	50.8211	98.3289
Class 2B-lplm	32.0	±5.2382	±0.6609	99.5190	99.5881	98.2307
Class 2B-lpsm	27.0	±1.5709	±0.2980	29.2195	29.1910	96.0560
Class 3A-lssm	20.0	±2.6734	±0.1752	50.8339	50.8211	98.3289
Class 3A-slsm	15.0	±1.5024	±0.0987	28.5654	28.5778	98.3993
Class 3A-llsm	17.0	±1.7185	±0.1227	32.6778	32.6598	98.4219
Class 3A-lslm	29.0	±4.8914	±0.3119	92.9974	93.0055	98.4170
Class 3A-lllm	14.5	±1.2099	±0.1484	22.9903	23.0709	98.1367

Fig. 14 through 19 shows the static force plots, the percent constant-force plots, the model force plots, the mean force plots, the median force plots, and the peak-to-peak force plots for all modified CFSMs for a 40% slider displacement. Results for a single frequency with a very low peak-to-peak force for all modified CFSMs have been summarized and tabulated in Table 10. The percent constant-force (PCF) may be obtained using the expression [14; 15]

$$\mathrm{PCF} = 100 \times \left(\frac{\min(\mathrm{F_{modeled}})}{\max(\mathrm{F_{modeled}})}\right) \quad (17)$$

Multiplying by a hundred gives the PCF as a percentage with 100% being perfectly constant. The PCF is very important because it measures the amount of variation between the minimum and maximum output force of the modified CFSMs. The maximum force is taken to be the maximum force throughout the percent displacement specified for the modified CFSMs. Due to the nature of the modified CFSMs, this force is usually located at the maximum deflection. The minimum force is defined similarly to the maximum force, and can generally be found at the smallest deflection. As a measure of goodness of fit, the relative error formula is given by

$$\mathrm{E} = \frac{|\mathrm{F_{modeled}} - \mathrm{F_{measured}}|}{|\mathrm{F_{measured}}|} \quad (18)$$

Where,

E = Relative error

$F_{modeled}$ = Average peak-to-peak force as predicted by the model

$F_{measured}$ = Average peak-to-peak force as observed during experiment

For better presentation, goodness of fit G_{fit} is cast as a percentage,

$$\mathrm{G_{fit}} = 100 \times (1 - \mathrm{E}) \quad (19)$$

Fig. 20 through 24 present the goodness of fit plots for the GMDM. The result shows how well the modeled force matches the measured force for each frequency tested. Also shown is the relative error when τ_{CF} and τ_{AF} are neglected in the modeled force calculations. Observe that the GMDM represents the modified CFSMs very well. Over the range of frequencies tested, the modeled force is within about 1% relative error of the measured force. The contribution of τ_{AF} in comparison to τ_{CF} as shown in the figures is more predominant than anticipated. This shows that the inclusion of τ_{AF} is very crucial to the dynamic model. This research work in conjunction with the research work of Lyon et al. [8]; Boyle [1]; Ugwuoke [13]; Ugwuoke, Abolarin and Ogwuagwu [14]; and Ugwuoke [15] further validates the usefulness of the PRBM as a dynamics modeling tool.

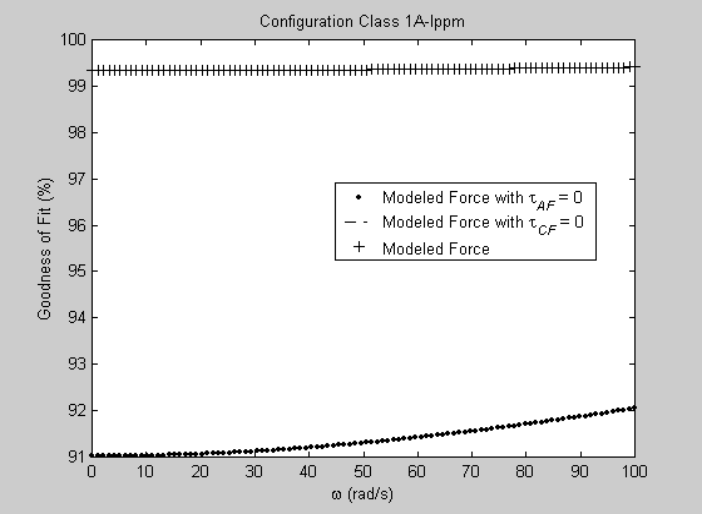

Fig. 20. Goodness of Fit of Modeled to Measured Force (Class 1A-lppm)

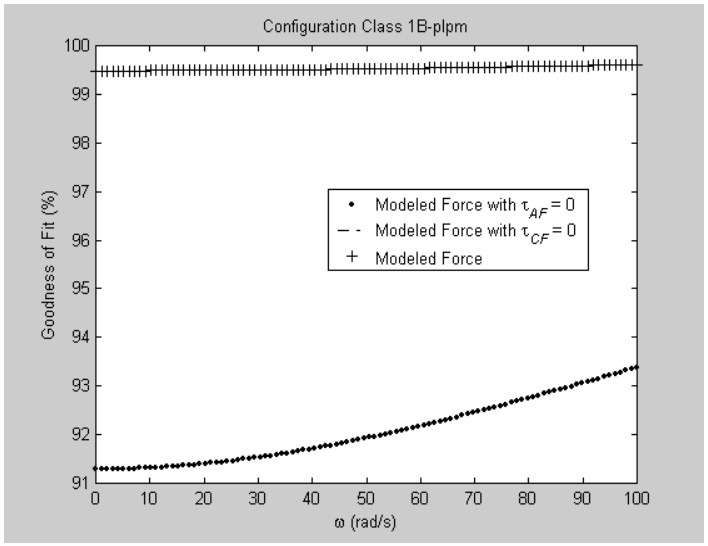

Fig. 21. Goodness of Fit of Modeled to Measured Force (Class 1B-plpm)

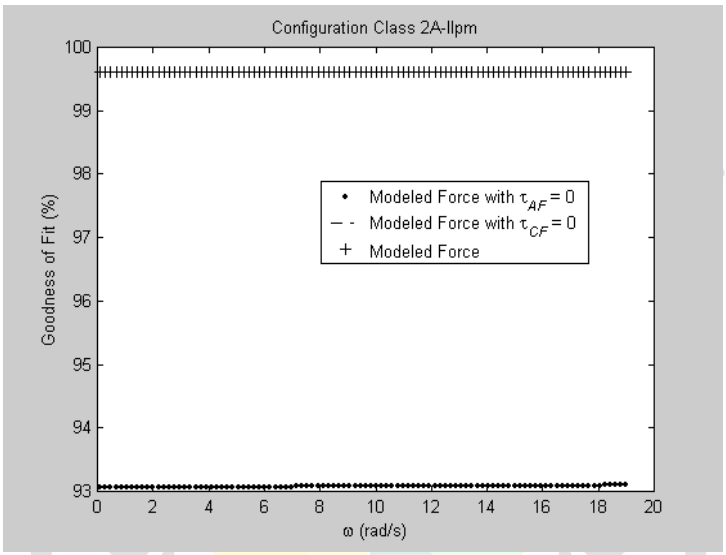

Fig. 22. Goodness of Fit of Modeled to Measured Force (Class 2A-llpm)

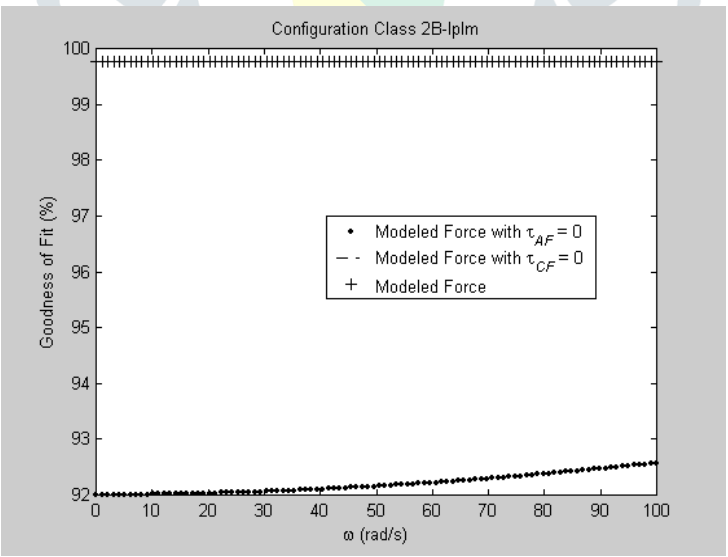

Fig. 23. Goodness of Fit of Modeled to Measured Force (Class 2B-lplm)

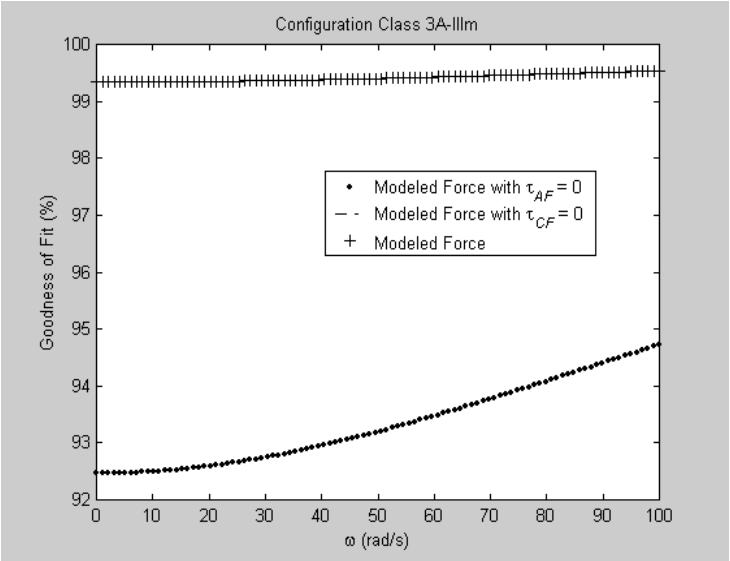

Fig. 24. Goodness of Fit of Modeled to Measured Force (Class 3A-lllm)

VI. Conclusion

This research addresses the desire to also understand the dynamic behavior of the Modified Configurations of Constant Force Slider Mechanisms (CFSMs). Based on the principle of Dynamic Equivalence, a Generalized Mathematical Dynamic Model (GMDM) was developed for all modified configurations of CFSMs developed. In the dynamic evaluation of the modified configurations of CFSMs, three useful plots were also analyzed, the mean force plot, the median force plot and the peak-to-peak force magnitude difference plot as a function of frequency for a 40% slider displacement. It was noticed that the curve in the peak-to-peak force plot first curves down, then sustains a linear range before it starts to increase. This very interesting phenomenon of the peak-to-peak force plot shows that there is a range of frequencies over which the modified configurations of CFSMs exhibits better constant-force behavior than they do statically. This better constant-force behavior is also likely due to inertial effects. Comparing the results obtained from experimentation with that obtained from the GMDM with inclusion of τ_{CF} and τ_{AF} shows a very good agreement as demonstrated by the goodness of fit plots. Over the range of frequencies tested, the results for the modeled force were within 1% of relative error of the measured force. The goodness of fit plots also revealed that the contribution of τ_{AF} in comparison to τ_{CF} is more predominant than anticipated which shows that the inclusion of τ_{AF} is very crucial to the GMDM. This research work in conjunction with other previous research work further validates the usefulness of the PRBM as a dynamics modeling tool. Depending on what attributes are most desirable; a wide frequency band with moderately low peak-to-peak force, a single frequency with very low peak-to-peak force, or some other similar effects, the modified configurations of CFSMs parameters can also be optimized to achieve the desired results.

References

[1] Boyle, C. L., 2001, “A Closed-Form Dynamic Model of the Compliant Constant-Force Mechanism using the Pseudo-Rigid-Body Model”, M.S. Thesis, Brigham Young University, Provo, Utah.

[2] Burns, R. H., 1964, “The Kinetostatic Synthesis of Flexible Link Mechanisms”, Ph.D. Dissertation, Yale University, New Haven, Connecticut.

[3] Evans, M. S. and Howell, L. L., 1999, “Constant-Force End-Effector Mechanism”, Proceedings of the IASTED International Conference, Robotics and Applications, Oct. 28-30, Santa Barbara, CA, USA, pp. 250-256.

[4] Howell, L. L., 2001, “Compliant Mechanisms”, John Wiley and Sons, New York.

[5] Howell, L. L., Midha, A., and Murphy, M.D, 1994, “Dimensional Synthesis of Compliant Constant-Force Slider Mechanisms”, Machine Elements and Machine Dynamics, DE, Vol. 71, pp. 509-515.

[6] Howell, L. L. and Midha, A., 1995, “Parametric Deflection Approximations for End-Loaded Large Deflection Beams in Compliant Mechanisms”, ASME Journal of Mechanical Design, Vol. 117, No. 1, pp. 156-165.

[7] Kota, S., Hetrick, J., Li, Z., and Saggere, L., 1999, “Tailoring Unconventional Actuators Using Compliant Transmissions: Design Methods and Applications”, IEEE/ASME Transactions on Mechatronics, Vol. 4, No. 4, December 1999, pp. 396-408.

[8] Lyon, S. M., Evans, M. S., Erickson, P. A., and Howell, L. L. (1997): Dynamic Response of Compliant Mechanisms Using the Pseudo-Rigid-Body Model. Proceedings of the 1997 ASME Design Engineering Technical Conferences, DETC97/VIB-4177.

[9] Millar, A. J., Howell, L. L., and Leonard, J. N., 1996, “Design and Evaluation of Compliant Constant-Force Mechanisms”, Proceedings of the 1996 ASME Design Engineering Technical Conferences and Computers in Engineering Conference, 96-DETC/MECH-1209.

[10] Murphy, M. D., Midha, A., and Howell, L. L., 1994, “Methodology for the Design of Compliant Mechanisms Employing Type Synthesis Techniques with Example”, Proceedings of the 1994 ASME Mechanisms Conference, DE, Vol. 70, pp. 61-66.

[11] Murphy, M. D., 1993, “A Generalized Theory for the Type Synthesis and Design of Compliant Mechanisms”, Ph.D Dissertation, Purdue University, West Lafayette, Indiana.

[12] Sandor, G. N. and Erdman, A. G., 1988, “Advanced Mechanism Design: Analysis and Synthesis”, Volume 2, Prentice-Hall, New Delhi, pp. 435-530.

[13] Ugwuoke, I. C., 2008, “A Simplified Dynamic Model for Constant-Force Compression Spring”, Leonardo Journal of Sciences, Issue 13, July-December 2008, 30-43.

[14] Ugwuoke, I. C., Abolarin, M. S., and Ogwuagwu, O. V., 2009, "Dynamic Behavioral Model Development for Constant-Force Compression Spring Electrical Contacts", Journal of Research in Engineering, 6(2), 76-85.
[15] Ugwuoke, I. C., 2010, "Dynamic Modeling and Simulation of Compliant Constant-Force Mechanisms", PhD Thesis, Department of Mechanical Engineering, Federal University of Technology, Minna, Nigeria.
[16] Weight, B. L., 2001, "Development and Design of Constant-Force Mechanisms", M.S. Thesis, Brigham Young University, Provo, Utah.